Protein import and oxidative folding in the mitochondrial intermembrane space of intact mammalian cells

Manuel Fischer[a], Sebastian Horn[a], Anouar Belkacemi[b], Kerstin Kojer[a], Carmelina Petrungaro[a], Markus Habich[a], Muna Ali[a], Victoria Küttner[c], Melanie Bien[a], Frank Kauff[d], Jörn Dengjel[c], Johannes M. Herrmann[e], and Jan Riemer[a]

[a]Cellular Biochemistry, [d]Molecular Phylogenetics, and [e]Cell Biology, University of Kaiserslautern, 67663 Kaiserslautern, Germany; [b]Experimental and Clinical Pharmacology and Toxicology, Saarland University, 66424 Homburg, Germany; [c]Freiburg Institute for Advanced Studies-LifeNet, ZBSA Center for Biological Systems Analysis, and BIOSS Centre for Biological Signaling Studies, University of Freiburg, 79108 Freiburg, Germany

ABSTRACT **Oxidation of cysteine residues to disulfides drives import of many proteins into the intermembrane space of mitochondria. Recent studies in yeast unraveled the basic principles of mitochondrial protein oxidation, but the kinetics under physiological conditions is unknown. We developed assays to follow protein oxidation in living mammalian cells, which reveal that import and oxidative folding of proteins are kinetically and functionally coupled and depend on the oxidoreductase Mia40, the sulfhydryl oxidase augmenter of liver regeneration (ALR), and the intracellular glutathione pool. Kinetics of substrate oxidation depends on the amount of Mia40 and requires tightly balanced amounts of ALR. Mia40-dependent import of Cox19 in human cells depends on the inner membrane potential. Our observations reveal considerable differences in the velocities of mitochondrial import pathways: whereas preproteins with bipartite targeting sequences are imported within seconds, substrates of Mia40 remain in the cytosol for several minutes and apparently escape premature degradation and oxidation.**

Monitoring Editor
Thomas D. Fox
Cornell University

Received: Dec 10, 2012
Revised: May 6, 2013
Accepted: May 8, 2013

INTRODUCTION

Disulfide bonds stabilize protein folds and complexes, regulate protein functions, and contribute to the distribution of proteins in specific cellular compartments. In eukaryotic cells cysteines are oxidized to disulfide bonds in two compartments that harbor dedicated enzymatic machineries—the endoplasmic reticulum and the intermembrane space of mitochondria (IMS; Stojanovski *et al.*, 2008; Riemer *et al.*, 2009). Disulfide bond formation in both compartments takes place by similar principles: an oxidoreductase that contains an oxidized dicysteine motif interacts with reduced substrates and introduces disulfide bonds within these substrates. Consequently, the oxidoreductase becomes reduced and is reoxidized by a sulfhydryl oxidase, which couples de novo disulfide bond formation ultimately to the electron acceptor oxygen using the cofactor flavin adenine dinucleotide (Stojanovski *et al.*, 2008; Riemer *et al.*, 2009).

Oxidative protein folding in the mitochondrial IMS presumably is coupled to protein import (oxidation-dependent import; Chacinska *et al.*, 2009; Riemer *et al.*, 2009; Herrmann and Riemer, 2010; Endo *et al.*, 2010; Sideris and Tokatlidis, 2010). The mechanism of disulfide bond formation has been characterized in molecular detail in *Saccharomyces cerevisiae* using purified proteins and isolated mitochondria. The oxidoreductase and the sulfhydryl oxidase of the IMS are the essential proteins Mia40 and Erv1, respectively (Lisowsky *et al.*, 2001; Chacinska *et al.*, 2004; Naoe

This article was published online ahead of print in MBoC in Press (http://www.molbiolcell.org/cgi/doi/10.1091/mbc.E12-12-0862) on May 15, 2013.

The authors declare no conflict of interest.

J.R. and M.F. designed the study and the experiments. All authors performed the experiments and analyzed and discussed the results. J.R. wrote the manuscript with input from M.F. and J.H.

Address correspondence to: Jan Riemer (jan.riemer@biologie.uni-kl.de).

Abbreviations used: AMS, 4-acetamido-4′-maleimidylstilbene-2,2′-disulfonic acid; BCNU, 1,3-bis(chloroethyl)-1-nitrosourea; CCCP, carbonyl cyanide *m*-chlorophenyl hydrazone; GSH, reduced glutathione; IMS, intermembrane space of mitochondria; MTS, mitochondrial targeting sequence; TCA, trichloroacetic acid; TCEP, Tris(2-carboxyethyl)phosphine.

et al., 2004; Mesecke *et al.*, 2005; Banci *et al.*, 2009). Proteins that follow the pathway for oxidation-driven import are typically <15 kDa and form simple helix-loop-helix structures in which the antiparallel helices are connected by two disulfide bonds. Larger IMS proteins are often synthesized with so-called bipartite presequences, which direct these proteins to the general matrix-targeting import pathway, from which they deviate into the IMS by a stop-transfer mechanism at the level of the inner membrane (Neupert and Herrmann, 2007; Chacinska *et al.*, 2009).

Substrates of the oxidation-dependent import pathway contain a Mia40-binding signal, also called MISS or ITS sequence, that is essential for their import into mitochondria (Milenkovic *et al.*, 2009; Sideris *et al.*, 2009). Mia40 and Erv1 transfer electrons via cytochrome *c* and cytochrome *c* oxidase to oxygen, from which water is produced (Allen *et al.*, 2005; Farrell and Thorpe, 2005; Bihlmaier *et al.*, 2007; Dabir *et al.*, 2007). At least in vitro, efficient Mia40-mediated protein oxidation relies on the presence of reduced glutathione (GSH; Bien *et al.*, 2010).

Basically all our knowledge of the mitochondrial disulfide relay is deduced from studies with mitochondria isolated from yeast cells. Only little is known about the mechanisms of disulfide bond formation in the mammalian IMS. The human homologues of Mia40 and Erv1 are Mia40 (also CHCHD4) and augmenter of liver regeneration (ALR; also growth factor erv1-like), respectively. Together Mia40 and ALR can mediate disulfide bond formation in vitro (Banci *et al.*, 2009; Daithankar *et al.*, 2009). Purified ALR can interact with cytochrome *c* or oxygen to become oxidized (Farrell and Thorpe, 2005). Upon Mia40 depletion in human tissue culture cells, the levels of selected disulfide-containing IMS proteins decrease (Hofmann *et al.*, 2005). Moreover, Mia40 and ALR can replace their yeast counterparts, implying functional homology of the mammalian and yeast pathways (Chacinska *et al.*, 2008; Di Fonzo *et al.*, 2009).

The absence of assays to assess disulfide bond formation in the IMS in intact cells prevented the investigation of oxidation-dependent import under physiological conditions. Here we establish an assay based on a pulse-chase approach coupled to a subsequent redox state determination and immunoprecipitation of specific proteins. The assay allows determination of protein oxidation in intact cells, which reveals half-time values of ~8 min. Thus preproteins remain in the cytosol for a considerable time, during which they are protected from degradation and unwanted oxidative folding. We also find evidence that it is not targeting to mitochondria or electron transfer from Mia40 that define the kinetics of the overall process but instead recognition and folding of substrates by Mia40. Moreover, we define the contributions of ALR and the cellular glutathione system to oxidative folding in the IMS. Surprisingly, we find that, contrary to previous results from experiments with isolated yeast mitochondria, oxidation-dependent import in intact cells is strongly dependent on the mitochondrial membrane potential, which reveals an unexpected connection between the energetic state of mitochondria and the oxidation-dependent protein import into mitochondria.

RESULTS

In intact cells the kinetics of oxidative protein folding in the mitochondrial IMS can be followed by an oxidation assay

Protein import into the IMS mainly has been assessed in the model system *S. cerevisiae* and by in vitro approaches. We aimed to investigate this pathway in intact mammalian cells. To this end, we established a pulse-chase immunoprecipitation approach coupled to redox-state determination ("oxidation assay"), which we applied to the twin-CX_9C protein Cox19. Cox19 contains four cysteine residues that, if present in their reduced form, are accessible to modification with 4-acetamido-4′-maleimidylstilbene-2,2′-disulfonic acid (AMS; Figure 1A, lane 1). Changes in the migration behavior of modified proteins in SDS–PAGE allow distinguishing between different redox forms of a protein. Cox19 is completely localized to mitochondria (Supplemental Figure S1), where the four cysteines form two disulfide bonds (Figure 1A, lane 3).

We performed the oxidation assay as follows (Figure 1B). Cells were radioactively labeled with [^{35}S]methionine for 5 min, followed by different chase times in medium containing nonradioactive methionine. The chase was stopped by rapid acidification using trichloroacetic acid (TCA), which prevents thiol–disulfide exchange reactions. Subsequently, proteins were modified by AMS. Finally, endogenous Cox19 was immunoprecipitated using a specific antibody and analyzed by SDS–PAGE and autoradiography. Using this assay, we found that newly synthesized Cox19 was almost completely reduced directly after the pulse and became oxidized during the subsequent chase with a half-time of 8 min (Figure 1C). Mature Cox19 (and thus nonradioactive protein) that was also precipitated in the assay was oxidized over the whole chase period (Figure 1D).

Whereas the number of twin-CX_3C proteins is conserved between *S. cerevisiae* and *Homo sapiens*, a recent in silico study (Cavallaro, 2010) identified 28 potential twin-CX_9C proteins in the human genome, compared with the 14 twin-CX_9C proteins in yeast. We extended this analysis and identified three additional potential twin-CX_9C proteins, bringing their total number in human cells to 31 (Figure 1E and Supplemental Table S1). Thus human cells harbor more than twice the number of twin-CX_9C proteins as yeast cells (Longen *et al.*, 2009). Many of these proteins contain additional cysteine residues outside the twin-CX_9C motif. To test whether the oxidation kinetics observed with Cox19 is also valid for proteins with different cysteine patterns, we performed the oxidation assay on three additional proteins: Cmc1 (cysteine pattern: CX_9CC-CX_9C-C), Cmc3 ($CX_9CX_9CX_9C$), and NDUFA8 (CX_9C-CX_9C-CX_9C-CX_9C; Figure 1E). To this end, we generated stable, inducible cell lines that express hemagglutinin (HA)-tagged variants of these proteins and compared the import with a cell line expressing HA-tagged Cox19. For all IMS-localized proteins investigated in this study (twin-CX_9C proteins, Mia40 variants, ALR, Smac) we used stable, inducible cell lines because transient or constitutive overexpression of the proteins resulted in their mislocalization to the cytosol (for the establishment of expression conditions and cellular localizations see Supplemental Figures S1–S3). The HA tag did not interfere with the localization of Cox19 to mitochondria, and we also found that the three selected twin-CX_9C proteins localized to mitochondria, indicating that these proteins are indeed twin-CX_9C proteins (Supplemental Figure S1). Of note, the tagged and overexpressed proteins became oxidized with comparable kinetics that was slightly slower than that of endogenous Cox19 (Figure 1F). The oxidation of NDUFA8 proceeded through a semioxidized intermediate (Figure 1F, 4 AMS bound) that is probably a form in which one twin-CX_9C motif has been fully oxidized, whereas the second one still is reduced. Due to its two twin-CX_9C motifs the kinetics of NDUFA8 oxidation to the fully oxidized protein proceeded only at about half the rate of Cox19. Taken together, we established an assay to follow the oxidation kinetics of IMS-localized, disulfide-containing proteins in intact cells. Because all twin-CX_9C proteins that we tested behaved in a similar way, we decided to focus in subsequent experiments on Cox19.

Oxidative folding in the mitochondrial IMS in intact cells is limited by the amount of Mia40

Oxidation of twin-CX_9C proteins appears to proceed relatively slowly. To elucidate whether the machinery that mediates disulfide

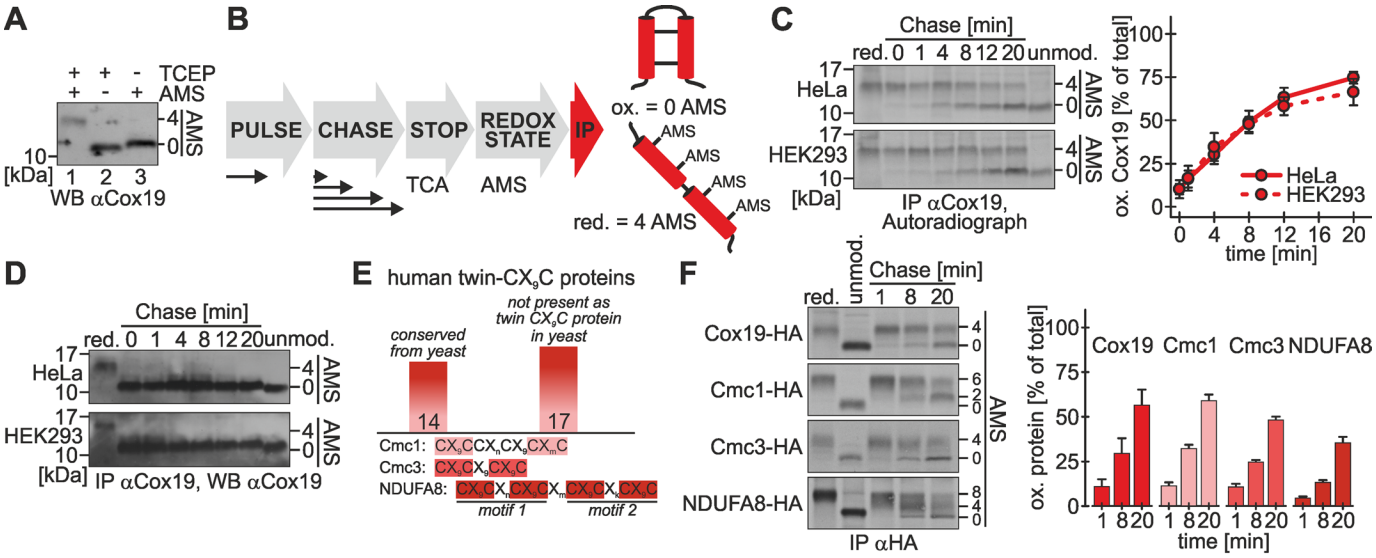

FIGURE 1: Oxidative folding of Cox19 proceeds with a half-time of 8 min in intact mammalian cells. (A) In intact cells Cox19 is oxidized. Cells were precipitated with TCA, and samples were treated with TCEP, TCEP plus AMS, or only AMS (steady state). The Cox19 redox state was analyzed by SDS–PAGE and immunoblotting (WB). (B) Scheme of the oxidation assay to follow oxidative folding in intact cells. Cells are pulse labeled for 5 min with [^{35}S]methionine and chased with cold methionine for different times. The chase is stopped by TCA precipitation, and then the lysate is treated with AMS to determine protein redox states, followed by IP against the protein of interest. Eluates are analyzed by Tris-Tricine-PAGE and autoradiography. Reduced Cox19 is modified with four AMS, whereas oxidized Cox19 remains unmodified. (C) Newly synthesized Cox19 becomes oxidized with a half-time of 8 min in HEK293 and HeLa cells. Experiments were performed as described in B, using an antibody against Cox19. Reported values are the mean of six independent experiments. (D) Mature Cox19 is oxidized during the duration of the entire oxidation assay. Experiments from C were analyzed by WB against Cox19. (E) The human twin-CX$_9$C protein family consists of 31 members, 14 of which are conserved from yeast, whereas 17 are novel additions in higher eukaryotes. For a complete list of the members of the twin-CX$_9$C family see Supplemental Table S1. Proteins of the twin-CX$_9$C family contain diverse cysteine motifs, exemplified by Cmc1, Cmc3, and NDUFA8. (F) Oxidation of Cmc1-HA, Cmc3-HA, and NDUFA8-HA can be followed using the oxidation assay. Experiments were performed as described in B, using an antibody against the HA epitope tag. The indicated proteins were expressed in stable, inducible cell lines (see Supplemental Figure S1 for their localization to mitochondria). Reported values are the mean of two independent experiments. Error bars in all graphs are means ± SD.

bond formation has only a limited capacity, we performed competition experiments in which we analyzed Cox19 oxidation while concomitantly overexpressing NDUFA8 (two twin-CX$_9$C motifs), Cmc3 (one twin-CX$_9$C motif), or Smac (import independent of Mia40), respectively. Whereas Smac overexpression did not impair Cox19 oxidation, the overexpression of both Cmc3 and NDUFA8 delayed the oxidation of Cox19 (Figure 2A). This suggests that twin-CX$_9$C proteins compete with each other for oxidation-dependent import, most likely at the level of the oxidoreductase Mia40.

To investigate the relevance of the levels of human Mia40 for protein import, we established the small interfering RNA (siRNA)–mediated knockdown of Mia40 (Supplemental Figure S2, A and B), as well as an overexpression protocol for Mia40 in stable, inducible cell lines (Supplemental Figure S2, C and D). Mia40 could be depleted to levels <10% compared with control siRNA–treated cells, and the levels of substrate proteins were lowered compared with control siRNA–treated cells (Supplemental Figure S2B). For Mia40 overexpression we used cells expressing either wild-type Mia40 (Mia40^{WT}) or a Mia40 variant that lacks the redox-active CPC motif (Mia40^{SPS}). Both proteins were overexpressed by ~20-fold and localized to mitochondria (Supplemental Figure S2, C and D).

Under conditions of Mia40 depletion, we found a strong impairment of Cox19 oxidation to ~20% of the rate found upon control siRNA treatment (Figure 2B). Conversely, overexpression of Mia40^{WT} increased the initial oxidation rate of Cox19 (Figure 2C), whereas overexpressed Mia40^{SPS} almost completely prevented the oxidation of Cox19 (Figure 2C). It has to be emphasized that overexpression of both Mia40 variants took place in cells that still contain endogenous Mia40 and that our overexpression protocol ensured that levels of endogenous Mia40 remained comparable in all cells (Supplemental Figure S2D). This indicates that Mia40^{SPS} functions as a dominant-negative mutant for Cox19 oxidation. Taken together, our results show that in vivo the levels of redox-active Mia40 are critical for Cox19 oxidation rather than the diffusion time of newly synthesized precursor proteins to mitochondria.

Our data could indicate that Cox19 and Mia40 interact for a prolonged time. Mia40–substrate complexes could be observed under steady-state conditions in intact yeast cells (Bottinger *et al.*, 2012). It remained unclear, however, whether these interactions are long lasting. To trace Mia40-Cox19 complexes in vivo, we pulse labeled newly synthesized proteins in cells stably expressing Cox19-HA and then performed an immunoprecipitation (IP) against Mia40 followed by a second IP on the eluate against HA (i.e., Cox19-HA). Under nonreducing conditions we detected a mixed Mia40-Cox19 dimer of ~30 kDa (Figure 2D, lane 2, arrowhead), which disappeared upon treatment with dithiothreitol (DTT; Figure 2D, lane 3, circle). After chase times of 20 min this dimer disappeared almost completely, indicating that the Mia40-Cox19 dimer represented a

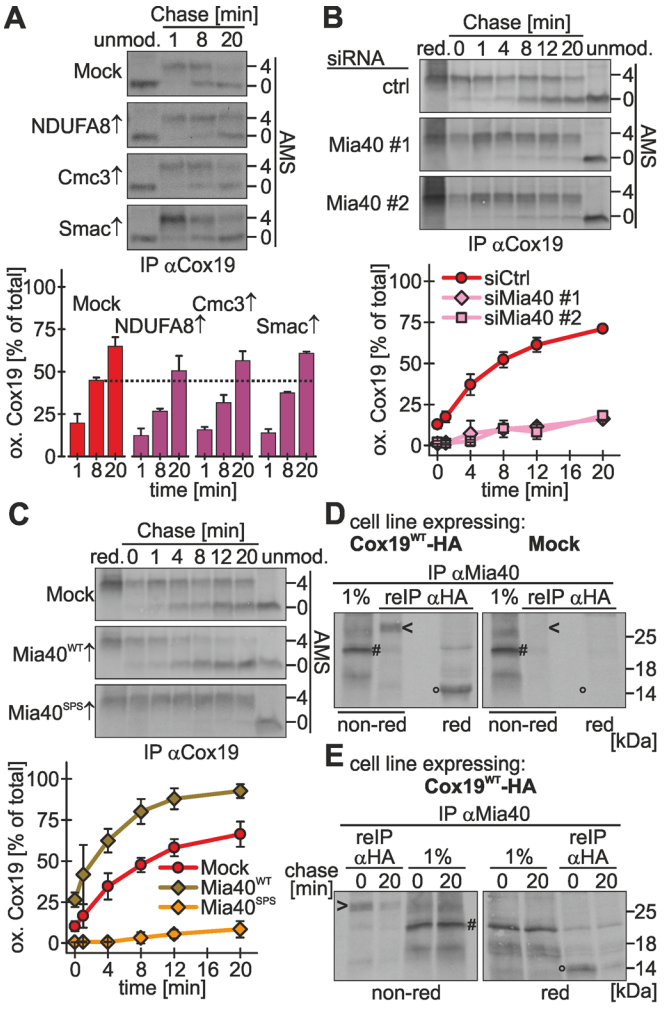

FIGURE 2: Mia40 is critical and limiting for oxidative folding in the IMS of intact mammalian cells. (A) Overexpression of twin-CX_9C proteins delays Cox19 oxidation. Experiments were performed as described in Figure 1B, using an antibody against Cox19, except that cells stably expressing different twin-CX_9C proteins or Smac-HA (a protein targeted to the IMS by a mitochondrial targeting signal) were induced 1 h before the experiment with doxycycline. Reported values are the mean of two independent experiments. (B) Oxidative folding is impaired in cells depleted of Mia40. Experiments were performed as described in Figure 1B, using an antibody against Cox19, except that 72 h before experiments cells were transfected with control siRNA or two different siRNAs directed against Mia40 (#1 and #2). Mia40 depletion was verified (Supplemental Figure S2A). Reported values are the mean of at least two independent experiments. (C) Overexpression of $Mia40^{WT}$ accelerates oxidative folding, and overexpression of a Mia40 active-site mutant ($Mia40^{SPS}$) impairs oxidative folding. Experiments were performed as described in Figure 1B, using an antibody against Cox19, except that cells stably expressing an empty vector (Mock), wild-type Mia40 ($Mia40^{WT}$) or an active-site mutant of Mia40 ($Mia40^{SPS}$) were induced 1 d before the experiment for 4 h with doxycycline. See Supplemental Figure S2C for localization of Mia40 variants to mitochondria. Reported values are the mean of at least two independent experiments. (D) Mia40 interacts with Cox19 via a mixed disulfide bond. Cells stably expressing Cox19-HA or an empty plasmid (Mock) were induced for 1 h and then radioactively pulse labeled for 4 h. Then thiol–disulfide exchange was inhibited by treatment with *N*-ethylmaleimide, cells were lysed using an SDS-containing buffer, and Mia40 was immunoprecipitated. One percent of this IP was loaded as control. Then a second IP with an antibody directed against the HA epitope was performed and analyzed by reducing and nonreducing SDS–PAGE and autoradiography. Arrowhead, disulfide-linked Mia40-Cox19 dimer; hash key, Mia40; circle, Cox19; red, reducing SDS–PAGE; non-red, nonreducing SDS–PAGE. (E) Mia40 interacts transiently with Cox19 during oxidation. Experiments were performed as in D, except that after the radioactive pulse, cells were chased with cold methionine for 0 or 20 min. Arrowhead, disulfide-linked Mia40-Cox19 dimer; hash key, Mia40; circle, Cox19; red, reducing SDS–PAGE; non-red, nonreducing SDS–PAGE. Error bars in all graphs are means ± SD.

reaction intermediate during Cox19 oxidation (Figure 2E, compare lanes 1 and 2).

Oxidative folding often is accompanied by misoxidation (i.e., generation of nonnative disulfide bonds) or the accumulation of trapped substrate–oxidoreductase complexes. In the endoplasmic reticulum reduced glutathione takes a prominent role in correcting these nonnative disulfide bonds (Chakravarthi *et al.*, 2006). We proposed a similar role for glutathione in oxidative folding in the yeast IMS based on in vitro reconstitution experiments (Bien *et al.*, 2010). The glutathione redox state in the IMS of human cells has not been systematically assessed. Thus we first applied a method using redox-sensitive, green fluorescent protein (roGFP)–based sensor proteins (Gutscher *et al.*, 2008) that we recently established (Kojer *et al.*, 2012) to investigate the glutathione pools of cytosol, IMS, and matrix. The glutathione redox potential in all three compartments was similarly reduced (Figure 3A), with values of –296, –292, and –289 mV for cytosol, IMS, and matrix, respectively. This again supports that protein oxidation in the IMS is not the consequence of changes in the redox environment compared with the cytosol but instead the consequence of an enzymatically catalyzed process. When glutathione reductase was inhibited with 1,3-bis(2-chloroethyl)-1-nitrosourea (BCNU) to deplete cells from reduced glutathione, a slightly more oxidized steady-state glutathione redox potential was observed in the matrix, and recovery after hydrogen peroxide treatment was strongly delayed in all three compartments (Figures 3, B–D), particularly in the IMS and the matrix (Figure 3, C and D).

Next we tested whether reduced glutathione facilitates oxidative folding by Mia40 and ALR. To this end, we treated cells with BCNU and applied the oxidation assay. Under these conditions we found a clear decrease of the Cox19 oxidation rate compared with control treatments (Figure 3E; similar results for Cmc1 and Cmc3, Supplemental Figure S2E). Cox19 is a substrate with a simple fold, and thus the beneficial influence of reduced glutathione on protein oxidation might be more prominent when analyzing more complex substrates. We do not know any Mia40 substrates with complex disulfide patterns. However, the twin-CX_9C protein NDUFA8 contains two twin-CX_9C motifs in its structure and thus might be suited to further investigate the role of the glutathione pool in oxidative folding. When we compared the oxidation kinetics of NDUFA8 in the presence and absence of BCNU, we again observed a clear delay of oxidative folding upon inhibition of the glutathione reductase (Figure 3F). Taking the results together, we have defined Mia40 as critical determinant of the oxidation rate in intact cells. Moreover, we have found that the reducing glutathione milieu contributes to the efficiency of oxidative folding in vivo.

ALR is critical for oxidative folding and competes with substrates for interaction to Mia40

To investigate the role of the human Erv1 homologue ALR, we established protocols for siRNA-mediated knockdown and

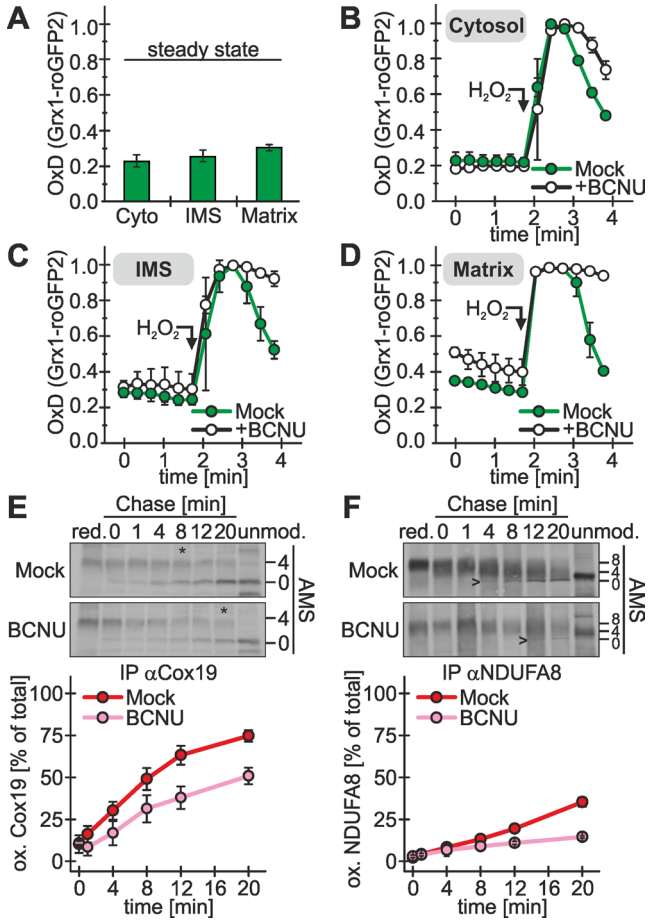

FIGURE 3: The reducing IMS glutathione pool contributes to efficient oxidative folding. (A) The IMS is as reducing as the cytosol. A redox-sensitive ratiometric fluorescent probe (Grx1-roGFP2; Gutscher *et al.*, 2008) was introduced into the cytosol and the mitochondrial IMS and the matrix of HEK293 cells. The stably expressed probe was induced 1 d before the experiment for 1 h with doxycycline. The degree of oxidation of the probe (OxD corresponding to the redox potential of the surrounding glutathione pool) was determined using a previously established fluorescence spectroscopic assay (Kojer *et al.*, 2012). Reported values are the mean of three independent experiments. (B–D) IMS, cytosol, and matrix exhibit a delayed recovery after oxidative shock upon incubation with glutathione reductase inhibitor. Experiments were performed as described in A. Cells were incubated for 1 h with 100 µM BCNU. To assess the dynamics of the glutathione pools in the different compartments, cells were incubated with 500 µM H_2O_2 (arrow), and deviation from and recovery to the steady state was followed in the cytosol (B), the IMS (C), and the matrix (D) with Grx1-roGFP2 probes targeted to the respective compartments. Reported values are the mean of three independent experiments. (E) Oxidative folding of Cox19 is delayed by glutathione reductase inhibition. Experiments were performed as described in Figure 1B, using an antibody against Cox19. Before the oxidation, assay cells were incubated with 100 µM BCNU for 1 h or left untreated (Mock). Asterisks indicate the time point at which half of the Cox19 protein is oxidized. Reported values are the mean of at least two independent experiments. (F) Oxidative folding of the complex twin-CX_9C protein NDUFA8 is delayed by glutathione reductase inhibition. Experiments were performed as described in E, using an antibody against the HA epitope tag. NDUFA8-HA expression was induced in stable cell lines 1 h before the experiment. Arrowheads indicate the time point at which fully oxidized NDUDFA8 becomes visible. Reported values are the mean of two independent experiments. Error bars in all graphs are means ± SD.

overexpression (Supplemental Figure S3, A–E). Although silencing depleted the levels of ALR to levels <10%, levels of cysteine-rich IMS proteins, including Mia40, were found unchanged, indicating that ALR levels are not as limiting for their biogenesis as are the levels of Mia40 (Supplemental Figure S3B). Overexpression in stable, inducible cell lines resulted in an increase of ALR levels by a factor of 10 (Supplemental Figure S3C). Upon depletion of ALR, the oxidation rate of Cox19 decreased to ~50% of control siRNA rates (Figure 4A). Surprisingly, also upon overexpression of ALR the oxidation rate of Cox19 decreased (Figure 4B). Using DTT titration experiments, we could exclude that this slower oxidative folding was caused by Mia40 overoxidation that might have impaired a potential isomerization function of Mia40 (Supplemental Figure S3F). Instead we found that ALR competes with substrates for binding to Mia40. When we assessed the interaction of Mia40 with Cox19 in the presence of different ALR levels, we observed that upon overexpression of ALR the amount of Cox19 bound to Mia40 was diminished compared with the control situation (Figure 4C, compare lanes 1 and 2). Consistently, we found that a larger fraction of endogenous Mia40 was bound to ALR upon ALR overexpression (Figure 4D, compare lanes 1 and 2). These findings are in line with in vitro data showing that ALR reoxidizes Mia40 by interacting with the substrate-binding cleft of Mia40 and that Mia40 only interacts with either ALR or its substrates (Banci *et al.*, 2011).

The final electron acceptor for the formation of disulfide bonds is molecular oxygen. To test whether modulations of the oxygen tension influence the kinetics of oxidation in the IMS, we investigated oxidative folding at 1 and 20% oxygen. Of interest, we did not observe a significant difference in the kinetics, indicating that oxidation-dependent import is not affected by changes in oxygen tension in this range (Figure 4E). This finding, together with the long interaction of substrates and Mia40, suggests that folding and not oxidation constitutes the rate-limiting step of oxidation-dependent import. Thus we propose that small changes in the oxidation kinetics do not result in changed rates of overall oxidation-dependent import if folding still proceeds more slowly than the oxidation step. Taking the results together, we find ALR to be a critical determinant of the oxidation rate. Its amounts have to be carefully balanced because too high as well as too low amounts of ALR result in reduced oxidative folding rates.

Oxidation-dependent protein import couples posttranslational translocation with oxidative folding

To test how the oxidation of Cox19 correlates with its translocation into mitochondria, we performed cell fractionations using digitonin after the pulse chase period (Figure 5A). Whereas we found the majority of Cox19 in the cytosolic fraction (~80%) directly after the radioactive pulse, after a 20-min chase the majority of Cox19 was present in the mitochondrial fraction (>60%; Figure 5B), suggesting that oxidation and import are kinetically coupled. Mature Cox19 was localized to mitochondria during the complete chase time.

This coupling was very evident in experiments in which Mia40 or ALR was silenced or overexpressed. Upon depletion of Mia40 and ALR, less Cox19 was found in the mitochondrial fraction after a 20-min chase than with control conditions (Figure 5C; also compare to Figures 2B and 4A). Conversely, overexpression of Mia40 led to higher Cox19 levels in mitochondria (Figure 5D). Of interest, overexpression of $Mia40^{SPS}$ resulted in a decreased accumulation of Cox19 in mitochondria (Figure 5D). However, this effect was not as strong as the inhibition of Cox19 oxidation by $Mia40^{SPS}$ (compare to Figure 2C). This indicates that a small amount of Cox19 is translocated to

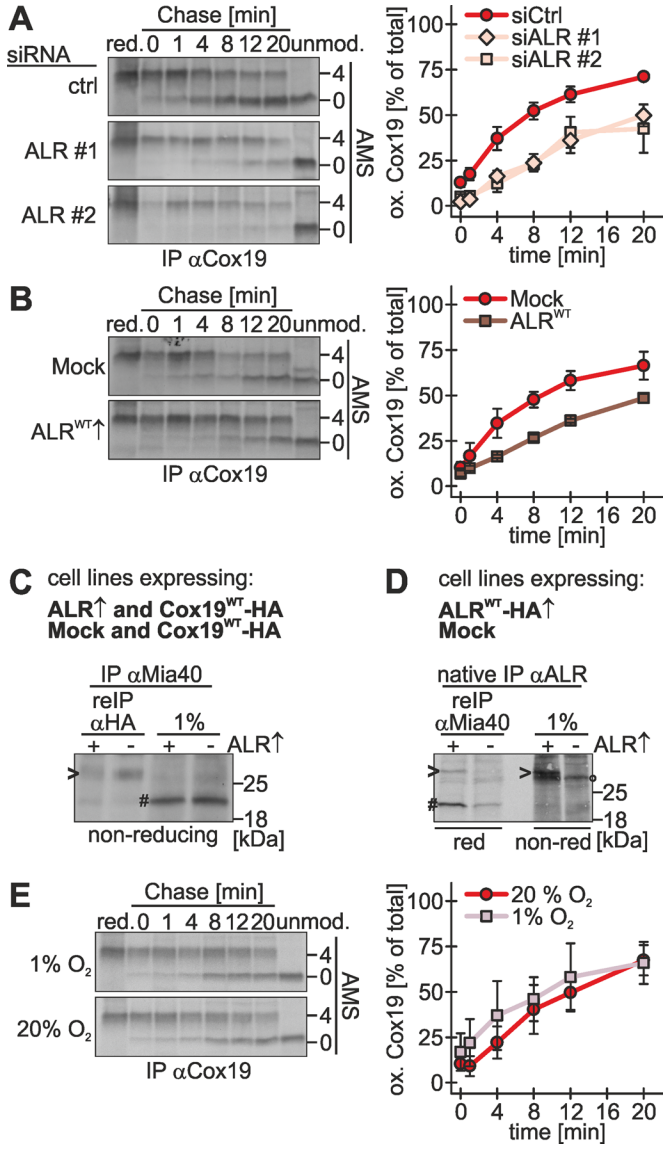

FIGURE 4: Oxidative folding depends on ALR and is not affected by changes in oxygen tension. (A) Oxidative folding is impaired in cells depleted of ALR. Experiments were performed as described in Figure 1B, using an antibody against Cox19, except that 72 h before experiments cells were transfected with control siRNA or two different siRNAs directed against ALR (#1 and #2). ALR depletion was controlled by immunoblot (Supplemental Figure S3A). Reported values are the mean of at least two independent experiments. (B) ALR overexpression delays Cox19 oxidation. Experiments were performed as described in Figure 1B, using an antibody against Cox19, except that cells stably expressing an empty vector (Mock) or wild-type ALR ($ALR40^{WT}$) were induced 1 d before the experiment for 1 h with doxycycline. See Supplemental Figure S3, D and E, for localization of ALR to mitochondria. Reported values are the mean of at least two independent experiments. (C) ALR competes with Cox19 for binding to Mia40. Experiments were performed as described in Figure 2D, except that Cox19-HA and ALR-HA, or Cox19-HA and an empty vector (Mock), were coexpressed. Arrowhead, disulfide-linked Mia40-Cox19 dimer; hash key, Mia40; red, reducing SDS–PAGE; non-red, nonreducing SDS–PAGE. (D) Overexpressed ALR sequesters Mia40. Cells stably expressing ALR-HA or an empty plasmid (Mock) was induced 1 d before the experiment for 1 h with doxycycline. Cells were radioactively pulse labeled for 4 h. Then thiol–disulfide exchange was inhibited by treatment with *N*-ethylmaleimide and cells were lysed under native conditions using a Triton X-100–containing buffer. ALR was immunoprecipitated using an antibody against ALR. One percent of this IP was loaded as control. Then a second IP with an antibody directed against Mia40 was performed and analyzed by reducing and nonreducing SDS–PAGE followed by autoradiography. Arrowhead, overexpressed ALR-HA; hash key, Mia40; circle, endogenous ALR; red, reducing SDS–PAGE; non-red, nonreducing SDS–PAGE. (E) Oxidative folding proceeds with similar kinetics at 20 and 1% oxygen. Experiments were performed as described in Figure 1B, using an antibody against Cox19, except that cells and buffers were incubated either at 20% oxygen or in a hypoxia chamber at 1% oxygen. Reported values are the mean of at least three independent experiments. Error bars in all graphs are means ± SD.

mitochondria independently of oxidation, presumably by noncovalent association with $Mia40^{SPS}$.

Taken together, our findings suggest a posttranslational import of Cox19 because full-length reduced Cox19 initially accumulates in the cytosolic fraction. Of note, nonimported Cox19 apparently was protected from cytosolic degradation since its levels remained stable in the cytosolic fraction over 20 min when import was prevented by silencing of Mia40 or ALR (see Figures 2, B and C, 4A, and 5, C and D). From the cytosolic pool, Cox19 was imported with kinetics that paralleled that of its oxidation (Figure 5E).

Oxidation-dependent import into the IMS is limited by the rate of oxidation and proceeds slowly compared with presequence-dependent import into the IMS

The notion that Cox19 import is slow became very apparent when its rate was compared with that of substrates containing mitochondrial presequences. We tested import of the presequence substrate Smac, which upon import into the IMS becomes proteolytically processed by the IMP protease (Burri *et al.*, 2005). Maturation leaves a truncated mature Smac, compared with a longer, nonimported form of this protein (Figure 6A). We used this difference in size to assess the import of Smac by a pulse-chase approach. Of note, in this assay we found that directly after 5 min of radioactive pulse, ~90% of Smac was already processed (Figure 6B), indicating that Smac import proceeds either cotranslationally or rapidly after its synthesis.

To further mechanistically dissect the oxidation-dependent import of Cox19 and compare it to presequence-mediated import, we uncoupled the import and oxidation of Cox19 by fusing Cox19 to the Smac presequence ($Smac^{MTS}$-Cox19-HA; MTS, mitochondrial targeting sequence; Figure 6C). This fusion protein localizes to mitochondria (Supplemental Figure S4) and is imported with similar rapidity as Smac-HA as judged by the processing of the presequence (Figure 6D). When we used the oxidation assay on $Smac^{MTS}$-Cox19-HA, we observed that oxidation proceeded with slightly faster kinetics as for Cox19-HA. It did not match, however, the rate of $Smac^{MTS}$-Cox19-HA processing (Figure 6E). Taken together, we find evidence that Cox19 oxidation is rate limiting for oxidation-dependent import and support for a model in which import of the substrate is tightly coupled to its initial interaction with Mia40.

Oxidation-dependent import of Cox19 is coupled to the mitochondrial membrane potential

Protein import by presequence-dependent pathways relies on the mitochondrial membrane potential (Figure 7A). One hallmark of oxidation-dependent protein import as deduced from protein import studies on isolated mitochondria is its independence from the membrane potential (Lutz *et al.*, 2003; Mesecke *et al.*, 2008). To assess a possible membrane potential dependence in intact cells, we

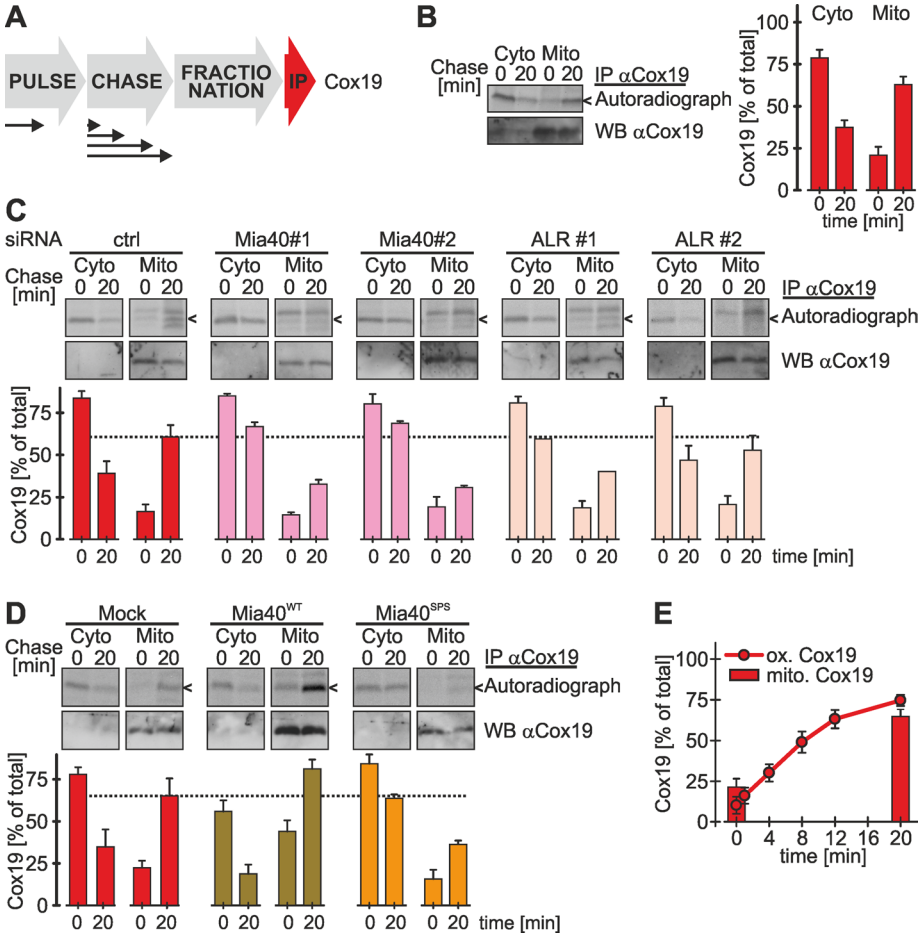

FIGURE 5: Oxidative folding is coupled to posttranslational protein import into the IMS. (A) Scheme for the experiment to assess the localization of freshly synthesized proteins. Cells are first pulse labeled for 5 min with [^{35}S]methionine and then chased with cold methionine for 0 or 20 min. At the end of the chase cells are transferred to ice and incubated with digitonin for 30 min to selectively permeabilize the plasma membrane. To separate the mitochondrial from the cytosolic fraction, lysates are centrifuged and proteins of interest are immunoprecipitated. Eluates are analyzed by SDS–PAGE and autoradiography. (B) Kinetics of Cox19 accumulation in mitochondria follows the kinetics of oxidative folding. Experiments were performed in HeLa cells as described in A, using an antibody against Cox19. Reported values are the mean of four independent experiments. To analyze localization of Cox19 at steady state, cells were treated as described in A and analyzed by immunoblotting against Cox19. (C) Mitochondrial accumulation of Cox19 is impaired upon depletion of Mia40 and ALR. Experiments were performed as described in A, using an antibody against Cox19, except that cells were transfected 72 h before the experiment with control siRNA or two siRNAs directed against Mia40 and ALR, respectively. To analyze localization of Cox19 at steady state, cells were treated as described in A and analyzed by immunoblotting against Cox19. Reported values are the mean of two independent experiments. (D) Overexpression of Mia40^{SPS} results in cytosolic accumulation of Cox19. Experiments were performed as described in A, using an antibody against Cox19, except that the analyzed cells overexpressed an empty plasmid (Mock), Mia40^{WT}, or Mia40^{SPS}. Expression of Mia40 variants was induced 24 h before the experiment for 4 h. To analyze localization of Cox19 at steady state, cells were treated as described in A and analyzed by immunoblotting against Cox19. Reported values are the mean of three independent experiments. (E) Mitochondrial accumulation and oxidation of Cox19 proceed with similar kinetics. The graphs from Figures 1C and 5B were combined for illustration. Error bars in all graphs are means ± SD.

dissolved the potential by applying carbonyl cyanide *m*-chlorophenyl hydrazone (CCCP) and valinomycin and subsequently followed the import of Smac and Cox19, respectively. As expected, Smac import was completely abolished under these conditions (Figure 7B). Of importance, Cox19 oxidation was also strongly impaired, indicating a direct or indirect dependence on the membrane potential (Figure 7C and Supplemental Figure S5A). In addition, under these conditions Cox19 remained stable in its reduced form. To exclude that the observed effect on Cox19 oxidation was limited to the CCCP/valinomycin treatment, we applied tyrphostin A9, a receptor tyrosine kinase inhibitor that has also been used to disrupt the mitochondrial membrane potential (Burger *et al.*, 1995; Sagara *et al.*, 2002). We again found decreased processing of Smac (Figure 7D), as well as delayed oxidation of Cox19 (Figure 7E). Because these findings are in contrast to observations made in in vitro import experiments with isolated yeast mitochondria, we adapted our pulse-chase import assay (Figure 1B) to yeast cells. Indeed, we also found an impairment of the oxidation of *Sc*Cox19 upon treatment with CCCP (Supplemental Figure S5B).

The membrane potential can regenerate after removal of CCCP/valinomycin (Head *et al.*, 2009; Tanaka *et al.*, 2010). We verified that MTS-mediated import is reestablished very rapidly even after treatment with high concentrations of CCCP (Supplemental Figure S5C). To test whether Cox19 that accumulated upon CCCP/valinomycin treatment is still import competent if the membrane potential is reestablished, we next performed a washout experiment (Figure 7F). To this end, we followed the oxidation of Cox19 in the presence of CCCP/valinomycin for 8 min and then washed the cells and further followed oxidative folding. Of importance, after washout the cytosolically accumulated Cox19 could be chased into the mitochondria, where it was oxidized (Figure 7F). The impaired oxidation kinetics upon CCCP/valinomycin treatment correlated with a decreased translocation into mitochondria (Supplemental Figure S5D). Of interest, the interaction between Mia40 and Cox19 was not disturbed upon depletion of the membrane potential (Supplemental Figure S5E), indicating a different reason for delayed oxidation-dependent import of Cox19 under these conditions. Taken together, the results show that depletion of the membrane potential reversibly inhibits Cox19 oxidation and import into mitochondria.

Oxidation-dependent import in primary cell lines

To this point we performed all experiments using immortalized cells. Next we wanted to address whether oxidation-dependent import proceeds similarly in primary nonimmortalized cells. To this end, we prepared primary mouse embryonic fibroblasts (MEFs) and performed the oxidation assay. Mouse Cox19 contains five instead of four cysteines, and thus mature mouse Cox19 migrates in its AMS-modified form slightly more slowly than

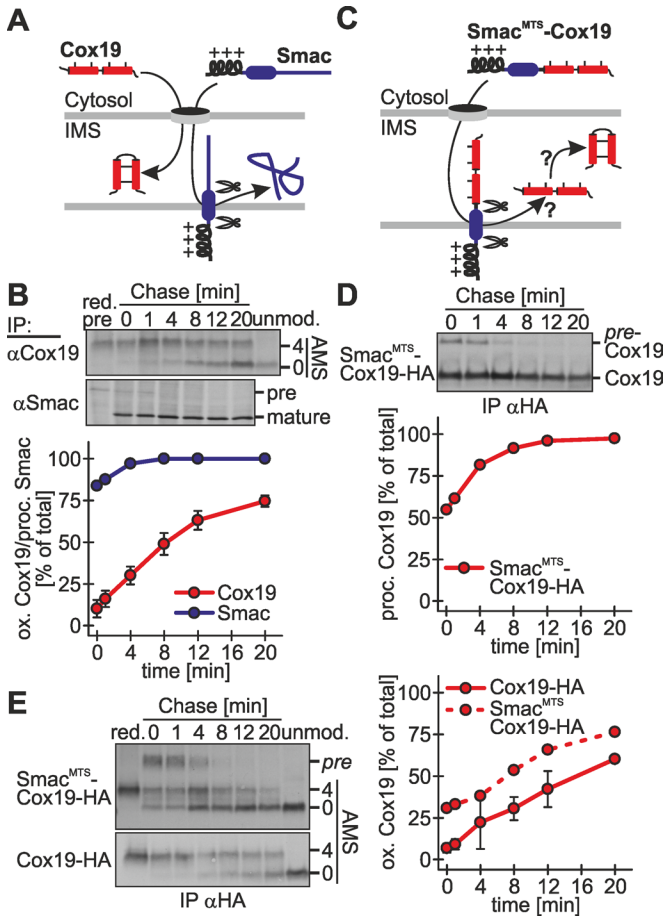

FIGURE 6: Oxidation-dependent protein import into the IMS proceeds more slowly than presequence-dependent protein import into the IMS. (A) Scheme of the maturation of Cox19 and Smac in the IMS. Smac and Cox19 are both localized to the IMS. Smac import relies on an amphipathic mitochondrial targeting sequence that becomes cleaved upon mitochondrial import. (B) Processing of Smac after cytosolic synthesis is a fast process. Experiments were performed as described in Figure 1B, using antibodies against Smac and Cox19, respectively. Reported values are the mean of at least two independent experiments. (C) Scheme of the processing of the fusion proteins Smac^{MTS}-Cox19-HA. For fast IMS import this fusion construct relies on the mitochondrial targeting sequence of Smac. The Smac targeting sequence becomes processed upon mitochondrial import. (D) Smac^{MTS}-Cox19-HA is processed with similar kinetics as endogenous Smac. Experiments were performed as described in Figure 1B, using an antibody against the HA-epitope tag. Samples were not modified with AMS. pre-Cox19, unprocessed Smac^{MTS}-Cox19-HA. Reported values are the mean of two independent experiments. (E) Oxidation of Smac^{MTS}-Cox19-HA proceeds with similar kinetics to oxidation of Cox19-HA. However, Smac^{MTS}-Cox19-HA initially is more oxidized than Cox19-HA. Experiments were performed as described in Figure 1B, using an antibody against the HA-epitope tag. Reported values are the mean of two independent experiments. Error bars in all graphs are means ± SD.

with the nonmodified protein (compare Figure 8A, lanes 1 and 2–4). The kinetics of Cox19 oxidation, however, was similar to that in HEK293 and HeLa cells (Figure 8A, top). Moreover, also in primary MEF cells we observed a dependence of oxidative folding on the membrane potential (Figure 8A, middle) and no changes in kinetics under conditions of low oxygen (Figure 8A, bottom). In summary, under physiological conditions, oxidation-dependent import follows a common set of principles that results in similar oxidation kinetics and depends on the mitochondrial membrane potential.

DISCUSSION

Here we established assays in intact mammalian cells to assess oxidation and import of mitochondrial IMS proteins. On the basis of data obtained with these assays, we propose the following model for oxidation-dependent import of Cox19 as it takes place in vivo (Figure 8B). This model likely also applies to other cysteine-rich Mia40 substrates in different cell types. According to our model, Cox19 accumulates after its synthesis in the cytosol, where it remains stable for several minutes, thereby being kept from degradation. Only after a considerable time is Cox19 threaded through the translocase of the outer membrane (TOM) channel into the IMS, where it encounters Mia40 and forms a disulfide-linked complex with the oxidoreductase. Overexpression of Mia40 strongly accelerates import and oxidation of Cox19, indicating that the concentration of Mia40 in the IMS is rate limiting for Cox19 translocation into mitochondria. This suggests that translocation into the IMS occurs only at TOM complexes that are in close contact to Mia40. Such a receptor-like function for yeast Mia40 has been proposed according to which Mia40 is associated with some TOM complexes via the structural IMS protein Fcj1/mitofilin (von der Malsburg *et al.*, 2011). Accordingly, overexpression of the redox-inactive Mia40^{SPS} mutant decreases protein translocation, as it reduces the chance of precursors to find a TOM pore that is in contact with a functional Mia40 protein. However, some Cox19 is still imported upon Mia40^{SPS} overexpression, although it does not become oxidized, indicating that noncovalent interactions between Cox19 and Mia40 can drive mitochondrial accumulation.

Upon interaction with Mia40, formation of both disulfides in Cox19 takes place. Of note, we do not observe Cox19 intermediates that only contain one disulfide bond, suggesting that both disulfide bonds are introduced in a rapid, potentially coordinated process. Mia40-mediated formation of disulfide bonds within Cox19 is most likely accompanied by a proofreading step that involves GSH. When we apply an inhibitor of glutathione reductase we find a clear reduction in the oxidation rate of Cox19, suggesting that GSH improves oxidation efficiency. This oxidation rate decrease becomes even more pronounced for NDUFA8, which contains four disulfide bonds in its mature form. Our data from intact cells are in line with data obtained by in vitro reconstitution approaches in which GSH accelerates oxidative folding by releasing trapped Mia40 from unproductive Mia40–substrate complexes (Bien *et al.*, 2010).

Translocation of newly synthesized Cox19 from the cytosol to mitochondria parallels the kinetics of Cox19 oxidation. On impairment of the machinery for oxidative folding by down-regulation of Mia40 or ALR or expression of the Mia40^{SPS} protein, oxidation and import are hampered. We thus conclude that import and oxidation are tightly coupled processes, which can be explained by our model, according to which import only occurs at TOM channels that are associated with Mia40.

On cytosolic accumulation, Cox19 is initially protected from premature oxidation and degradation. We propose that this stabilization also takes place during normally proceeding import of Cox19. Accordingly, Cox19 that accumulates in the cytosol due to a dissolved membrane potential is still import competent, as it becomes oxidized upon reestablishment of the membrane potential. This finding also strongly supports the notion that Cox19 import proceeds posttranslationally from a cytosolic pool of Cox19 precursors in intact cells. That this cytosolic pool might be a point of regulation

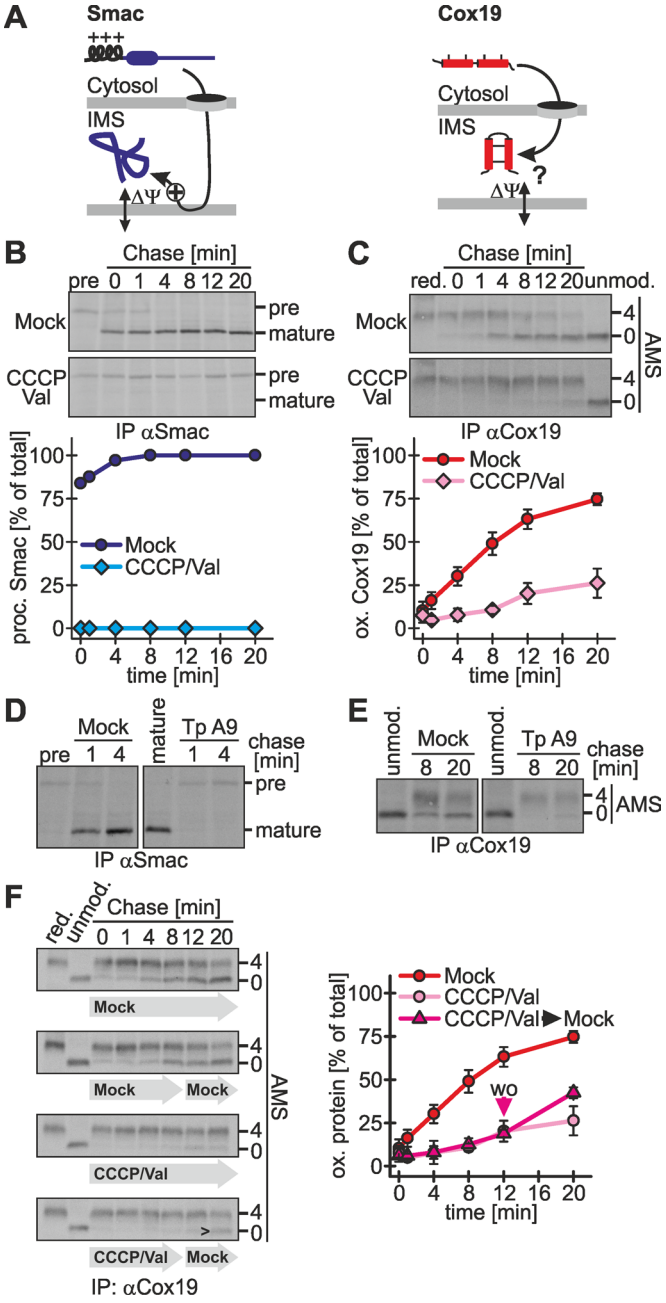

FIGURE 7: Oxidation-dependent import depends on the mitochondrial membrane potential. (A) Scheme for the membrane potential dependence of Smac and Cox19. Because Smac relies on a mitochondrial targeting sequence, its import depends on the membrane potential. It is not clear whether the membrane potential influences IMS import of Mia40-dependent substrates such as Cox19. (B) Smac import is coupled to the mitochondrial membrane potential. Experiments were performed as described in Figure 1B, using an antibody against Smac, except that cells were either Mock-treated or treated with 2 μM CCCP and 1 μM valinomycin. Val, valinomycin. Reported values are the mean of two independent experiments. (C) Cox19 import depends on the mitochondrial membrane potential. Experiments were performed as described in B, using an antibody against Cox19. Val, valinomycin. Reported values are the mean of at least two independent experiments. (D, E) Cox19 oxidation is impaired by treatment with tyrphostin A9 (Tp A9). Experiments were performed as described in Figure 1B, using antibodies against Smac (D) and Cox19 (E), respectively. Cells were either mock-treated or incubated with 1 μM tyrphostin A9. (F) The block in Cox19 import upon depletion of the mitochondrial membrane potential is reversible. Experiments were performed as described in Figure 1B, using an antibody against Cox19. Cells were either Mock-treated or incubated with valinomycin and CCCP. After 8 min, chase cells were washed with buffer and for the remaining 12 min of the chase time incubated with chase medium or chase medium containing valinomycin and CCCP. Val, valinomycin; wo, washout of CCCP/Val. Reported values are the mean of two independent experiments. The arrowhead indicates the appearance of oxidized Cox19 after washout of CCCP and valinomycin. Error bars in all graphs are means ± SD.

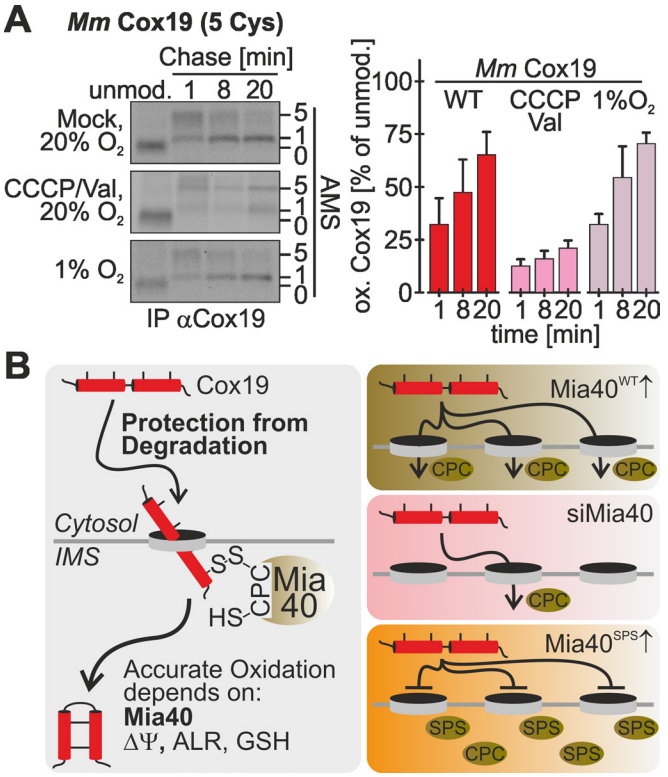

FIGURE 8: Mitochondrial import proceeds with similar kinetics in primary mouse embryonic fibroblasts. (A) Experiments on primary mouse embryonic fibroblasts were performed as described in Figure 1B, using an antibody against human Cox19 that also recognizes mouse Cox19. Cells were exposed to different oxygen tensions, as well as to a treatment with CCCP and valinomycin (Val). Reported values are the mean of at least three independent experiments. Error bars are means ± SD. (B) Model of Cox19 import into mammalian mitochondria. Oxidation-dependent import of Cox19 in mammalian cells depends on ALR, glutathione, the mitochondrial membrane potential, and Mia40. On the basis of our data, we propose that endogenous Mia40 is placed in a position where it optimally recognizes incoming proteins. From this position it likely is replaced by Mia40^{SPS}, which therefore serves as a dominant-negative mutant for protein oxidation.

is supported by recent data obtained with the yeast system that indicate that the cytosolic thioredoxin system contributes to maintaining a reduced redox state of cytosolic precursors (Durigon *et al.*, 2012). In addition, another study in yeast demonstrated that the available amounts of cytosolic precursors are modulated by the proteasome (Bragoszewski *et al.*, 2013).

In comparison to other pathways of mitochondrial protein import, oxidation-dependent import appears to proceed considerably more slowly. Smac, which contains a cleavable mitochondrial targeting

sequence, is almost completely imported after the initial radioactive pulse, whereas Cox19 import proceeds over the entire 20-min chase period. It is important to note that, although Smac was processed and imported within a short time frame, this does not mean that the protein also became folded during this time. When we uncoupled oxidation and import of Cox19 by equipping the protein with the mitochondrial targeting sequence of Smac, we observed a fast processing of the presequence as for Smac but after an initial "jump" in the extent of oxidation, a slow oxidation rate of Cox19 comparable to that of wild-type Cox19. This indicates that it is not targeting to mitochondria that is limiting for oxidation-dependent import but recognition and oxidative folding by Mia40. It also explains why import and oxidation appear to be tightly coupled processes.

One hallmark of oxidation-dependent import into isolated mitochondria is its independence of the mitochondrial membrane potential (Lutz *et al.*, 2003; Mesecke *et al.*, 2005). This is in contrast to substrates relying on mitochondrial targeting sequences for mitochondrial import. Using our oxidation assay in intact cells, we also found a strong dependence of Cox19 import on the mitochondrial membrane potential. The inhibition of import is reversible, as removal of the chemicals restores the functionality of the pathway for oxidative protein folding. This also strongly supports the notion that in intact cells import of Cox19 can proceed posttranslationally. Eukaryotic cells contain many mitochondria, which can differ considerably in membrane potential (Exner *et al.*, 2012; Rugarli and Langer, 2012; Youle and van der Bliek, 2012). The prerequisite of a high membrane potential and the stable nature of cytosolic precursor proteins imply that precursors might be predominantly imported into highly energized mitochondria, so that mitochondria with functional genomes might be preferred over those that carry mitochondrial DNA mutations. In the future, it will be exciting to further analyze oxidation-dependent import in living mammalian cells and study mitochondrial biogenesis in the context of propagating cells.

MATERIALS AND METHODS

Plasmids, cell lines, siRNAs, and antibodies

For plasmids and cell lines used in this study see Supplemental Tables S2 and S3. For the generation of stable, inducible cell lines the HEK293 cell line–based Flp-In™ T-REx™ -293 cell line was used with the Flp-In™ T-REx™ system (Invitrogen, Carlsbad, VA). For preparation of MEFs and the used siRNAs and antibodies see Supplemental Materials and Methods.

Assay to assess protein oxidation in intact cells (oxidation assay)

Cells were starved with cysteine- and methionine-free medium (Sigma-Aldrich, St. Louis, MO) for 15 min at 37°C. Newly synthesized proteins were pulse labeled for 5 min at 37°C with cysteine- and methionine-free medium containing [^{35}S]methionine at a concentration of 200 µCi/ml (PerkinElmer, Waltham, MA). Pulse labeling was stopped by removing the medium and adding chase medium containing 20 mM methionine. The chase was performed for variable times at 37°C, when it was stopped by adding ice-cold 8% TCA. TCA precipitation was performed by centrifugation at 13,000 × *g* for 15 min and washing with 5% ice-cold TCA. Protein precipitates were dissolved in modification buffer (0.2 M Tris, pH 7.5, 6 M urea, 10 mM EDTA, 2% SDS). Samples were modified with a final AMS concentration of 15 mM for 1 h at room temperature. Reduced controls were treated with a 2 mM Tris(2-carboxyethyl)phosphine (TCEP; final concentration) for 5 min at 96°C before AMS modification; oxidized controls were untreated. After modification samples were filled to 250 µl using lysis buffer A (30 mM Tris-Cl, pH 8, 100 mM NaCl, 5 mM EDTA, 2% SDS) and incubated for 5 min at 96°C. Then 750 µl of lysis buffer B (30 mM Tris-Cl, pH 8, 100 mM NaCl, 5 mM EDTA, 2.5% Triton X-100) was added and the mixture incubated at 4°C for 1 h. Samples were cleared by centrifugation at 25,000 × *g* for 1 h. The supernatant was subjected to immunoprecipitations with antibodies conjugated to protein A–Sepharose beads at 4°C overnight under gentle shaking. The samples were washed four times using lysis buffer C (30 mM Tris-Cl, pH 8, 100 mM NaCl, 5 mM EDTA, 1% Triton X-100) and once using lysis buffer D (30 mM Tris-Cl, pH 8, 100 mM NaCl, 5 mM EDTA). Proteins were eluted by adding Laemmli buffer (2% SDS, 60 mM Tris, pH 6.8, 10% glycerol, 0.0025% bromphenolblue) to the dried beads and subsequent boiling for 5 min at 95°C. Samples were analyzed by Tris-Tricine PAGE and autoradiography.

Assay to assess posttranslational import (organelle distribution assay)

The experiment was performed as the oxidation assay with the following modifications. The chase was stopped by incubating cells in ice cold fractionation buffer (20 mM 4-(2-hydroxyethyl)-1-piperazineethanesulfonic acid [HEPES], pH 7.4, 250 mM sucrose, 50 mM KCl, 2.5 mM MgCl, 1 mM dithiothreitol [DTT], 0.005% digitonin). Cells were incubated in this buffer for 30 min at 4°C. Samples were fractionated by centrifugation at 1000 × *g* for 5 min into a cytosolic and mitochondrial fraction. The latter was dissolved in trypsin buffer (20 mM HEPES, pH 7.4, 250 mM sucrose, 50 mM KCl, 2.5 mM MgCl, 1 mM DTT, 25 µg/ml trypsin) and incubated for 20 min at 4°C. TCA 50% was added to the samples to a final concentration of 8%. TCA precipitation was followed directly by immunoprecipitations. Samples were analyzed by SDS–PAGE and autoradiography.

Measurement of the glutathione redox potential

The expression of cytosolic and IMS- and matrix-localized Grx1-roGFP2 (Gutscher *et al.*, 2008) in stable, inducible cell lines was induced with doxycycline for 1 h at 1 d before the experiment. Measurements were performed as described (Kojer *et al.*, 2012). Cells were detached from a 10-cm dish and washed twice with phosphate-buffered saline, and 5×10^6 cells were resuspended in 500 µl of measurement buffer (0.1 M NaCl, 2 mM sorbitol, 0.1 M Tris-HCl, pH 7.4). Fluorescence measurements were performed with an FP6500 spectrofluorometer (Jasco, Tokyo, Japan) at 30°C with constant stirring. Spectra were recorded using excitation wavelengths from 390 to 500 nm (bandwidth ± 1.5–2.5 nm) and an emission wavelength of 511 nm (bandwidth ± 1.5–5 nm). Measurements were performed in a quartz cuvette (light path 5 mm; Hellma Analytics, Müllheim, Germany). Cells were monitored for 4 min and after 2.5 min H_2O_2 was added to a final concentration of 500 µM. For BCNU incubation cells were treated with 100 µM BCNU for 1 h at 37°C before the experiment.

Chemical treatments

Membrane potential was depleted by using 2 µg/ml CCCP, 1 µg/ml valinomycin, or 1 µg/ml tyrphostin A9 (all Sigma-Aldrich) for 15 min. Glutathione reductase was inhibited by using 0.1 mM BCNU for 1 h. DTT treatment in living cells was done by adding DTT to the chase medium in various concentrations (0.1, 0.25, 0.5, 1, 2, 5, 10 mM).

ACKNOWLEDGMENTS

We thank Veit Flockerzi and Heidi Löhr (Saarland University, Homburg, Germany) for help with MEF isolation and valuable discussions. We thank Vera Nehr and Andrea Trinkaus for technical assistance. This study was supported by the Deutsche Forschungsgemeinschaft (RI2150/1-1) and the Research Initiative for Membrane Transport.

REFERENCES

Allen S, Balabanidou V, Sideris DP, Lisowsky T, Tokatlidis K (2005). Erv1 mediates the Mia40-dependent protein import pathway and provides a functional link to the respiratory chain by shuttling electrons to cytochrome c. J Mol Biol 353, 937–944.

Banci L, Bertini I, Calderone V, Cefaro C, Ciofi-Baffoni S, Gallo A, Kallergi E, Lionaki E, Pozidis C, Tokatlidis K (2011). Molecular recognition and substrate mimicry drive the electron-transfer process between MIA40 and ALR. Proc Natl Acad Sci USA 108, 4811–4816.

Banci L, Bertini I, Cefaro C, Ciofi-Baffoni S, Gallo A, Martinelli M, Sideris DP, Katrakili N, Tokatlidis K (2009). MIA40 is an oxidoreductase that catalyzes oxidative protein folding in mitochondria. Nat Struct Mol Biol 16, 198–206.

Bien M, Longen S, Wagener N, Chwalla I, Herrmann JM, Riemer J (2010). Mitochondrial disulfide bond formation is driven by intersubunit electron transfer in Erv1 and proofread by glutathione. Mol Cell 37, 516–528.

Bihlmaier K, Mesecke N, Terziyska N, Bien M, Hell K, Herrmann JM (2007). The disulfide relay system of mitochondria is connected to the respiratory chain. J Cell Biol 179, 389–395.

Bottinger L, Gornicka A, Czerwik T, Bragoszewski P, Loniewska-Lwowska A, Schulze-Specking A, Truscott KN, Guiard B, Milenkovic D, Chacinska A (2012). In vivo evidence for cooperation of Mia40 and Erv1 in the oxidation of mitochondrial proteins. Mol Biol Cell 23, 3957–3969.

Bragoszewski P, Gornicka A, Sztolsztener ME, Chacinska A (2013). The ubiquitin-proteasome system regulates mitochondrial intermembrane space proteins. Mol Cell Biol 33, 2136–2148.

Burger AM, Kaur G, Alley MC, Supko JG, Malspeis L, Grever MR, Sausville EA (1995). Tyrphostin AG17, [(3,5-di-tert-butyl-4-hydroxybenzylidene)-malononitrile], inhibits cell growth by disrupting mitochondria. Cancer Res 55, 2794–2799.

Burri L, Strahm Y, Hawkins CJ, Gentle IE, Puryer MA, Verhagen A, Callus B, Vaux D, Lithgow T (2005). Mature DIABLO/Smac is produced by the IMP protease complex on the mitochondrial inner membrane. Mol Biol Cell 16, 2926–2933.

Cavallaro G (2010). Genome-wide analysis of eukaryotic twin CX9C proteins. Mol Biosyst 6, 2459–2470.

Chacinska A, Guiard B, Muller JM, Schulze-Specking A, Gabriel K, Kutik S, Pfanner N (2008). Mitochondrial biogenesis, switching the sorting pathway of the intermembrane space receptor Mia40. J Biol Chem 283, 29723–29729.

Chacinska A, Koehler CM, Milenkovic D, Lithgow T, Pfanner N (2009). Importing mitochondrial proteins: machineries and mechanisms. Cell 138, 628–644.

Chacinska A, Pfannschmidt S, Wiedemann N, Kozjak V, Sanjuan Szklarz LK, Schulze-Specking A, Truscott KN, Guiard B, Meisinger C, Pfanner N (2004). Essential role of Mia40 in import and assembly of mitochondrial intermembrane space proteins. EMBO J 23, 3735–3746.

Chakravarthi S, Jessop CE, Bulleid NJ (2006). The role of glutathione in disulphide bond formation and endoplasmic-reticulum-generated oxidative stress. EMBO Rep 7, 271–275.

Dabir DV, Leverich EP, Kim SK, Tsai FD, Hirasawa M, Knaff DB, Koehler CM (2007). A role for cytochrome c and cytochrome c peroxidase in electron shuttling from Erv1. EMBO J 26, 4801–4811.

Daithankar VN, Farrell SR, Thorpe C (2009). Augmenter of liver regeneration: substrate specificity of a flavin-dependent oxidoreductase from the mitochondrial intermembrane space. Biochemistry 48, 4828–4837.

Di Fonzo A *et al.* (2009). The mitochondrial disulfide relay system protein GFER is mutated in autosomal-recessive myopathy with cataract and combined respiratory-chain deficiency. Am J Hum Genet 84, 594–604.

Durigon R, Wang Q, Ceh Pavia E, Grant CM, Lu H (2012). Cytosolic thioredoxin system facilitates the import of mitochondrial small Tim proteins. EMBO Rep 13, 916–922.

Endo T, Yamano K, Kawano S (2010). Structural basis for the disulfide relay system in the mitochondrial intermembrane space. Antioxid Redox Signal 13, 1359–1373.

Exner N, Lutz AK, Haass C, Winklhofer KF (2012). Mitochondrial dysfunction in Parkinson's disease: molecular mechanisms and pathophysiological consequences. EMBO J 31, 3038–3062.

Farrell SR, Thorpe C (2005). Augmenter of liver regeneration: a flavin-dependent sulfhydryl oxidase with cytochrome c reductase activity. Biochemistry 44, 1532–1541.

Gutscher M, Pauleau AL, Marty L, Brach T, Wabnitz GH, Samstag Y, Meyer AJ, Dick TP (2008). Real-time imaging of the intracellular glutathione redox potential. Nat Methods 5, 553–559.

Head B, Griparic L, Amiri M, Gandre-Babbe S, van der Bliek AM (2009). Inducible proteolytic inactivation of OPA1 mediated by the OMA1 protease in mammalian cells. J Cell Biol 187, 959–966.

Herrmann JM, Riemer J (2010). The intermembrane space of mitochondria. Antioxid Redox Signal 13, 1341–1358.

Hofmann S, Rothbauer U, Muhlenbein N, Baiker K, Hell K, Bauer MF (2005). Functional and mutational characterization of human MIA40 acting during import into the mitochondrial intermembrane space. J Mol Biol 353, 517–528.

Kojer K, Bien M, Gangel H, Morgan B, Dick TP, Riemer J (2012). Glutathione redox potential in the mitochondrial intermembrane space is linked to the cytosol and impacts the Mia40 redox state. EMBO J 31, 3169–3182.

Lisowsky T, Lee JE, Polimeno L, Francavilla A, Hofhaus G (2001). Mammalian augmenter of liver regeneration protein is a sulfhydryl oxidase. Dig Liver Dis 33, 173–180.

Longen S, Bien M, Bihlmaier K, Kloeppel C, Kauff F, Hammermeister M, Westermann B, Herrmann JM, Riemer J (2009). Systematic analysis of the twin cx(9)c protein family. J Mol Biol 393, 356–368.

Lutz T, Neupert W, Herrmann JM (2003). Import of small Tim proteins into the mitochondrial intermembrane space. EMBO J 22, 4400–4408.

Mesecke N, Bihlmaier K, Grumbt B, Longen S, Terziyska N, Hell K, Herrmann JM (2008). The zinc-binding protein Hot13 promotes oxidation of the mitochondrial import receptor Mia40. EMBO Rep 9, 1107–1113.

Mesecke N, Terziyska N, Kozany C, Baumann F, Neupert W, Hell K, Herrmann JM (2005). A disulfide relay system in the intermembrane space of mitochondria that mediates protein import. Cell 121, 1059–1069.

Milenkovic D, Ramming T, Muller JM, Wenz LS, Gebert N, Schulze-Specking A, Stojanovski D, Rospert S, Chacinska A (2009). Identification of the signal directing Tim9 and Tim10 into the intermembrane space of mitochondria. Mol Biol Cell 20, 2530–2539.

Naoe M, Ohwa Y, Ishikawa D, Ohshima C, Nishikawa S, Yamamoto H, Endo T (2004). Identification of Tim40 that mediates protein sorting to the mitochondrial intermembrane space. J Biol Chem 279, 47815–47821.

Neupert W, Herrmann JM (2007). Translocation of proteins into mitochondria. Annu Rev Biochem 76, 723–749.

Riemer J, Bulleid N, Herrmann JM (2009). Disulfide formation in the ER and mitochondria: two solutions to a common process. Science 324, 1284–1287.

Rugarli EI, Langer T (2012). Mitochondrial quality control: a matter of life and death for neurons. EMBO J 31, 1336–1349.

Sagara Y, Ishige K, Tsai C, Maher P (2002). Tyrphostins protect neuronal cells from oxidative stress. J Biol Chem 277, 36204–36215.

Sideris DP, Petrakis N, Katrakili N, Mikropoulou D, Gallo A, Ciofi-Baffoni S, Banci L, Bertini I, Tokatlidis K (2009). A novel intermembrane space-targeting signal docks cysteines onto Mia40 during mitochondrial oxidative folding. J Cell Biol 187, 1007–1022.

Sideris DP, Tokatlidis K (2010). Oxidative protein folding in the mitochondrial intermembrane space. Antioxid Redox Signal 13, 1189–1204.

Stojanovski D, Muller JM, Milenkovic D, Guiard B, Pfanner N, Chacinska A (2008). The MIA system for protein import into the mitochondrial intermembrane space. Biochim Biophys Acta 1783, 610–617.

Tanaka A, Cleland MM, Xu S, Narendra DP, Suen DF, Karbowski M, Youle RJ (2010). Proteasome and p97 mediate mitophagy and degradation of mitofusins induced by Parkin. J Cell Biol 191, 1367–1380.

von der Malsburg K *et al.* (2011). Dual role of mitofilin in mitochondrial membrane organization and protein biogenesis. Dev Cell 21, 694–707.

Youle RJ, van der Bliek AM (2012). Mitochondrial fission, fusion, and stress. Science 337, 1062–1065.